PERGAMON

Micron 34 (2003) 351–358

micron

www.elsevier.com/locate/micron

Whole-mount sections displaying microvascular and glandular structures in human uterus using multiphoton excitation microscopy

F. Manconi[a,*], E. Kable[b], G. Cox[b], R. Markham[a], I.S. Fraser[a]

[a]*Department of Obstetrics and Gynaecology, Queen Elizabeth II Research Institute for Mothers and Infants, The University of Sydney, Sydney, NSW 2006, Australia*
[b]*Electron Microscope Unit, The University of Sydney, Sydney, NSW 2006, Australia*

Received 12 November 2002; revised 11 July 2003; accepted 31 July 2003

Abstract

There has been considerable interest over many years in the precise structural relationships between microvessels and secretory glands in human endometrium. However, microcirculatory networks have rarely been studied in three-dimensions (3D) using modern computerised technologies, this has been partly due to the late arrival of suitable endothelial cell markers. This study was designed to develop a technique to visualize and to reveal the relationships between microvessels, their glandular environment and epithelial boundaries in 3D, using endometrium from human hysterectomy biopsies. Specimens were carefully selected from women with conditions unlikely to affect the microvascular networks. Monoclonal antibodies (mouse anti-human CD 34 and goat anti-mouse fluorescein (FITC)) were used to visualize the microvessels, and polyclonal antibodies (rabbit anti-human keratin and goat anti-rabbit tetramethylrhodamine (TRITC)) were used to visualize the glandular structures. The samples were studied with a Leica multiphoton system using a titanium–sapphire laser (excitation 800 nm with pulses in the 200 fs range) to obtain a stack of two-dimensional (2D) images to a minimal focus depth of 120 μm. The initial data sets acquired were volume rendered using the integrated software of the Leica system to produce 3D images. This software allowed for the acquisition of data sets from the microscope and for an observational morphological assessment to be made, but was limited in preparing the data for any quantitative analysis. The additional use of ImarisBasic 3.1 visualization software allowed for an observational morphological assessment but also included numerous tools for data manipulation.

Keywords: Three-dimensional reconstruction; Microvascular; Endometrium; Multiphoton excitation microscopy; Immunofluorescence; Second harmonic imaging; Vibratome; Free float; Whole mount

1. Introduction

The uterus is a flattened, pear-shaped, hollow organ situated deep in the pelvis of the human female (Fig. 1). During pregnancy, it is the organ that enlarges dramatically to hold the unborn developing child. Suspended in the pelvis, it lies with the base directed upward and forward and the cervix directed slightly backward. In the non-pregnant condition, the uterus averages 7.5 cm in length, 5 cm in width, and 4 cm in thickness. Although the uterus is a muscular organ, it has a lining of soft glandular material, the endometrium, which thickens during and after ovulation, preparatory to receiving a fertilized ovum. If fertilization does not occur, this lining breaks down and is partially shed from the body in a process known as menstruation.

1.1. Associated endometrial structures

The endometrial epithelium consists of a monolayer of cuboidal cells that cover the interior of the endometrium. The endometrium is primarily specialised to allow embryo implantation, whilst also acting as a reproductive tract secretory mucosal barrier, providing continuous protection against pathogens that gain access to the uterine cavity (Simón et al., 2002). Endometrial glands can either be simple or branched tubular shapes, and may be coiled in the deeper portions; the glands secrete mucus, glycogen, and a range of proteins and lipids. The remainder of the endometrial tissue mainly consists of loose or dense and

* Corresponding author. Tel.: +612-9351-3844; fax: +612-9351-4560.
E-mail address: fmanconi@obsgyn.usyd.edu.au (F. Manconi).

0968-4328/$ - see front matter © 2003 Elsevier Ltd. All rights reserved.
doi:10.1016/j.micron.2003.07.002

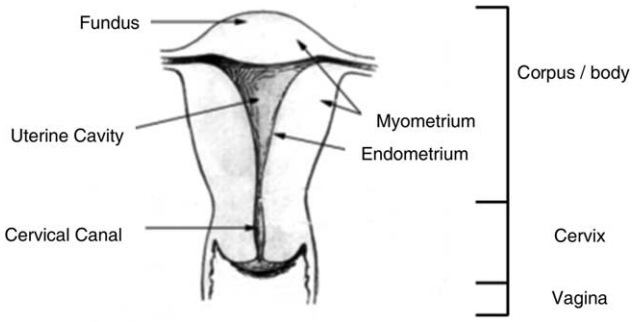

Fig. 1. Diagram of an opened uterus with landmark points.

highly specialised stromal cells, immunologically—competent cells and connective tissue.

1.2. Endometrial vasculature structures

The regulation of vasculature development is an important aspect of the growth and maturation of the endometrium. The gross morphology of the endometrial vascular bed has been well documented. The uterine and ovarian arteries branch-off to form between 6 and 10 arcuate arteries (so called because they run along a semicircular 'arc' around the uterus). These penetrate through the stratum vasculare (a layer of large blood vessels located between the inner and outer layers of smooth muscle) of the myometrium. The myometrium is the muscular layer of the uterus and is composed of a thick inner circular layer and a thinner outer longitudinal layer of smooth muscle. The arcuate arteries then branch to form the radial arteries (Markee, 1940; Ramsey, 1989; Ferenczy, 1994). Further branching occurs just inside the endometrial–myometrial interface, these arteries then branch at right angles to form short straight basal arterioles (anastomosing) which supply the basal layer of the endometrium. As the main branch of the radial arteries continues towards the endometrial epithelium, it becomes highly coiled and is referred to as a spiral arteriole (terminal), which supplies the functional layer of the endometrium. Endometrial tissue of an approximate surface area of 4–9 mm^2 is supplied by each spiral artery (Bartelmez, 1933), branching of the spiral arteries occurs throughout the functional layer to become numerous precapillaries and capillaries. About two-thirds into the functional layer, the vessels supply a subsurface capillary network, which contains many fenestrated capillaries just beneath the luminal epithelial surface. The subsurface capillary network also includes thin-walled dilated units called lacunae. The lacunae may also occur in the venous system, which drains the endometrium (Smith, 2002). A schematic diagram illustrating the blood supply to the two layers of the endometrium—basalis and functionalis is shown in Fig. 2.

There are numerous important gaps that still exist in our knowledge of the luminal epithelium, stroma and vasculature of human endometrium (Dockery et al., 2000). Current knowledge of the structure and function of microvessels in normal tissue is limited and an understanding of the 3D relationships between capillaries, spiral arteries, lymphatics, glands and surface epithelium is critical to the understanding of the disturbed angiogenesis and microvessel morphology which occur in some menstrual bleeding disorders.

Computer-generated 3D reconstruction of organs and tissue has become a powerful tool for increasing our comprehension of the anatomical and functional relationships between microscopic structures. This is particularly important for a tissue such as endometrium which is one of the most remarkable tissues in the body given its ability to undergo cyclical growth, maturation and partial shedding each month and also its potential to adapt to and nurture a pregnancy. Disturbances of microvessel structure and function are likely to underlie spontaneous menstrual bleeding disorders and breakthrough bleeding secondary to steroidal hormone therapy (Livingstone and Fraser, 2002). The use of 3D microscopical imaging should greatly help in conceptualizing some of the changing microanatomical relationships between glandular and microvascular structures.

Multiphoton Excitation Microscopy (MPE) (Peticolas et al., 1963; Denk et al., 1990) which is a development of fluorescence microscopy and Laser Scanning Confocal Microscopy (LSCM) (Wilson and Sheppard, 1984), has established itself as a valuable tool for obtaining high resolution images, and 3D reconstruction has proven to be an even more useful complement to the single-photon excitation confocal predecessor (Straub and Hell, 1998). MPE is particularly useful in the biological field because it can be used to probe delicate living cells and tissues without damaging the sample, and has a greater sample penetration and reduced photobleaching effect of marker dyes than LSCM. One of the main advantages of using MPE microscopy with respect to LSCM is the improved visual penetration into the sample and the ability to assess the morphology of tissue three-dimensionally throughout the volume of the specimen (Gerritsen and De Grauw, 1999).

Our initial experiments with MPE were carried out as a development of a long term interest in the 3D tissue architecture of human endometrium (Blackwell and Fraser, 1981, 1988; Manconi et al., 2001; Simbar et al., submitted).

2. Materials and methods

2.1. Tissue samples

Endometrial samples used for the study were selected from patients of reproductive age who underwent a hysterectomy in the King George V and Royal Prince Alfred Hospitals, Sydney, Australia. The Ethics Review Committees of the Central Sydney Area Health Service and

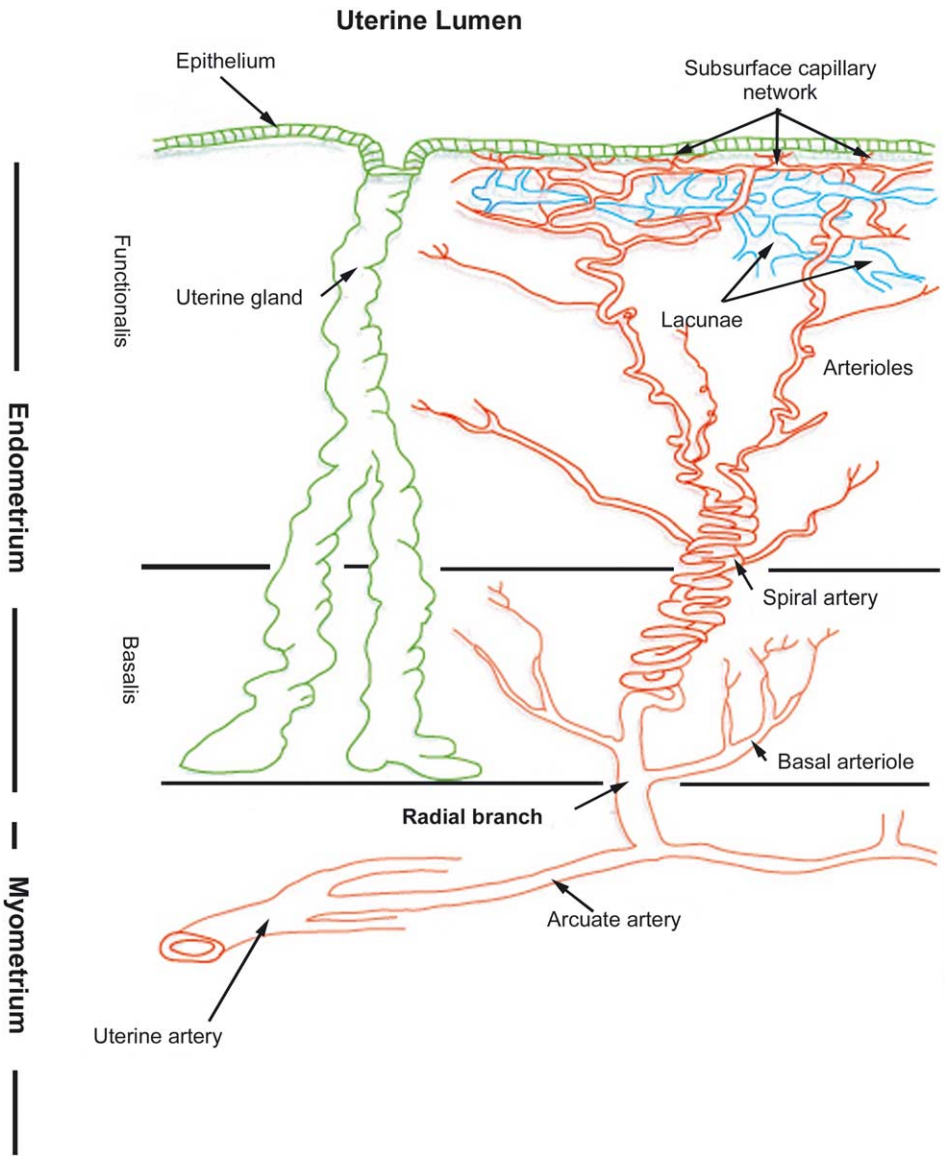

Fig. 2. The coiled endometrial spiral arteries originate from the myometrial arcuate arteries and have connections with the subsurface capillary network that includes thin-walled dilated units called lacunae. The lacunae may also occur in the venous system, which drains the endometrium. Ross, M.H., (1985). In: Ross, M.H., Reith, E.J. (Eds.), Histology: A Text and Atlas. Harper and Row, New York, p. 676. Reproduced with permission.

the University of Sydney approved collection of the samples for research purposes. Samples were only included if subjects had no specific gynaecological disease and had not undergone recent hormonal treatment. Endometrial samples were blindly assessed by a specialist gynaecological pathologist and accurately dated by the conventional criteria of Noyes, Hertig and Rock (Noyes et al., 1950).

2.2. Vibratome sectioning

Human uterine strips were fixed in 10% neutral buffered formalin and sectioned to an approximate thickness of 100 μm using a vibratome 1000 Classic (The Vibratome Company, St Louis, MO, USA). The principle of the vibratome is a vibrating blade intersecting the specimen underneath the surface of a physiological liquid bath, which lubricates the cut; this allows sectioning without freezing or embedding. The creation of artefacts, the alteration of morphology, the destruction of enzyme activities, and other deleterious effects that are inherent in freezing or embedding procedures are avoided.

2.3. Pretreatment

The pretreatment of the thick sections served two purposes; it allowed for the antibodies (CD 34 and Keratin) and fluorochromes (FITC and TRITC) to penetrate deeply and evenly into the thick section, and also it reduced the autofluorescence (Lee et al., 1997). Briefly, all sections were pretreated for 4 h at room temperature with an aqueous 3% sodium deoxycholate solution. The samples were then rinsed several times with distilled water and were further

pretreated with 0.01% pepsin in 0.01N HCl for 1.5 h at room temperature. The samples were rinsed several times with distilled water and a final rinse with 0.05 M Tris buffered saline (TBS) (pH 7.4).

Examination by both light and electron microscopy of the tissue fixed with 10% neutral buffered formalin and pretreated with sodium deoxycholate and then with pepsin in HCl indicated that the tissue and cellular architecture was not altered by this process.

2.4. Immunofluorescence

Monoclonal antibodies, mouse anti-human haematopoietic progenitor cell, CD 34 (M7165, DAKO, Corporation, Carpinteria, USA), was diluted 1:800 and incubated for 72 h at 4 °C. Fluorescein labelled goat anti-mouse (F-2761, Molecular Probes, Inc., Eugene, OR, USA), was diluted 1:800 and incubated for 24 h at 4 °C, were used to visualize the microvessels. Polyclonal antibodies rabbit anti-human keratin (A0575, DAKO Corporation, Carpinteria, USA), was diluted 1:800 and incubated for 72 h at 4 °C. Tetramethylrhodamine labelled goat anti-rabbit (T-2769, Molecular Probes, Inc., Eugene, OR, USA), diluted 1:800 and incubated 24 h at 4 °C, were used to visualize the glandular structures. Each incubation step was followed by two 15 min rinses in TBS pH 7.6, unless otherwise stated. Slides were mounted using fluorescent mounting medium (S3023, DAKO Corporation, Carpinteria, USA).

2.5. Microscopy

The microscope used was a Leica DMIRBE inverted stand equipped with a Leica TCS2-MP confocal system (Leica Laserteknik, Mannheim, Germany) and Coherent Mira tuneable pulsed titanium sapphire laser (Coherent Laser Group, Santa Clara, CA, USA). Excitation wavelengths from 925 to 760 nm were used, with pulses in the 100–200 fs range. Wavelengths were checked with a Rees spectrum analyser and pulse width with an APE autocorrelator. The microscope is equipped with dual photomultiplier transmitted light detectors, with dichroic mirrors dividing the detectable spectrum (380–680 nm) at either 505 or 560 nm; further selection was accomplished with the use of barrier filters in either or both channels. An identical dual detection unit was mounted behind the objective lens to act as a non-descanned two-photon excited fluorescence (TPF) detector. The specimens were observed using an objective lens PL FLUOTAR 25 × /0.75 Oil PH2 (Leica, Microsystems AG, Wetzlar, Germany). The TPF images were collected automatically as frame by frame sequential series. Single sections and 3D stacks were acquired.

2.6. Three-dimensional reconstruction

Once the data sets had been collected it was necessary to process them using a method appropriate to the type of information to be visually extracted. An MPE data set can either be processed as a series of 2D slices (optical sections) or the complete volume can be rendered as a whole using the Leica confocal integrated software of the TCS2-MP. This software allowed for the acquisition of the data sets from the microscope and for an observational morphological assessment.

Third party visualization software ImarisBasic 3.1 (Bitplane, AG Scientific Solutions, Zurich, Switzerland) was used and is a volume rendering program, the software accepts stacks of registered 2D images and creates 3D projections from any viewpoint. Tools included in the suite are for 2D and 3D measurements of individual isosurfaces and groups, it also allows for 2D slice viewing and movie loop generation. The 3D images can then be displayed as either solid or transparent structures.

The viewing of an image rotating on a computer monitor or saved as an Audio/Video Interleaved format file to be later played back on a computer gave a clear understanding of the 3D relationships of glandular and microvascular structures. This provided excellent visual cues to the shapes and inter-relationships of the different structures. Use of single computer printouts or photographs of the 3D image rarely provided an impression of the three-dimensionality of the structure. An orthogonal (also known as orthographic) projection is a way of providing a 2D graphic view of an object in which the projecting lines are drawn at right angles to the plane of projection. In so doing this type of presentation appears to give the impression of 3D, as demonstrated in Section 3.

3. Results

We have developed MPE through a series of stages where it can now be applied to precisely examine the 3D relationships between microvascular, glandular and epithelial structures within human endometrium at different stages of the menstrual cycle and in abnormal situations. The series of images presented here demonstrates the application of this technique to the study of different microstructures within human endometrium.

Illustrated in Fig. 3 is an orthogonal projection of a surface view of early secretory phase endometrium, which is 100 μm thick in the *z*-direction and the tissue appears to have been sectioned tangentially through an endometrial gland. The surface epithelium consists of a monolayer of cuboidal cells that lines the uterine lumen and is in continuity with the glandular epithelial cells, which are generally similar. The epithelial surface clearly shows a genuine fold (a), (from a uterine segment taken at hysterectomy which allows for the accurate shape of the endometrium to be retained, unlike samples derived from dilatation and curettage (D&C) or biopsy which tend to distort the architecture of the endometrium). Complex interconnecting capillary networks are formed just beneath

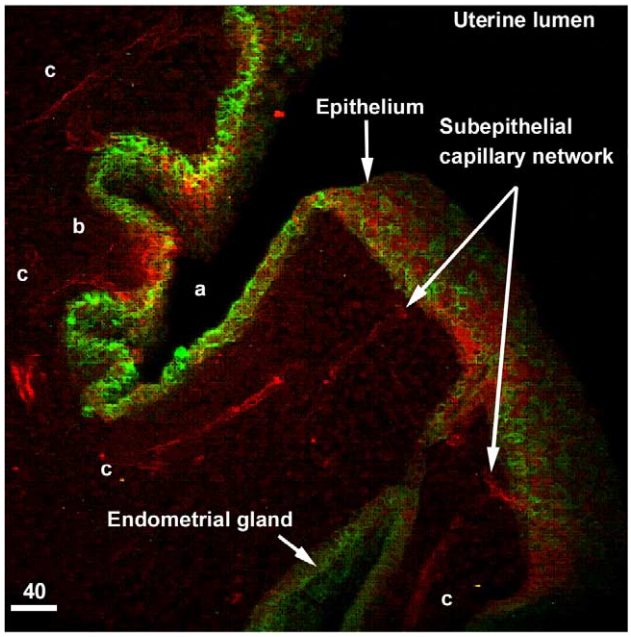

Fig. 3. An orthogonal projection, illustrating the surface layer of the endometrium. Mouse anti-human haematopoietic progenitor cell (CD34) and Fluorescein labelled goat anti-mouse were used to visualise the microvessels (red). Rabbit anti-human keratin and Tetramethylrhodamine labelled goat anti-rabbit were used to visualise the glandular structures (green). Scale = 40 μm.

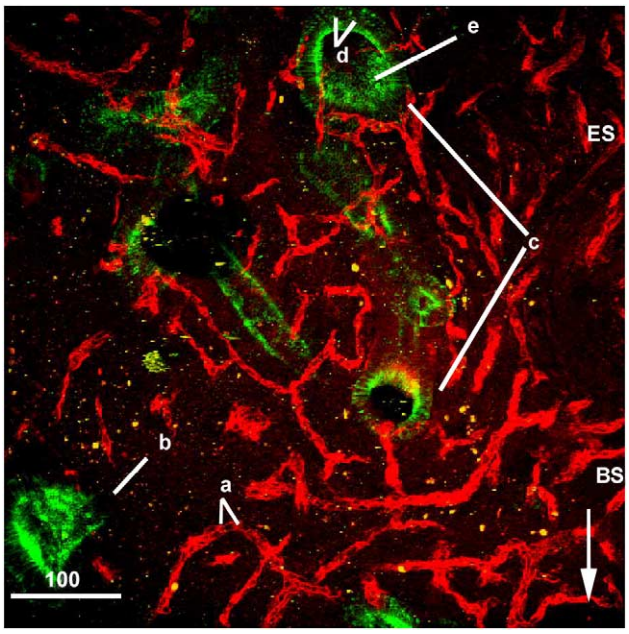

Fig. 4. An orthogonal projection, illustrating microvascular (red) and glandular structures (green) in endometrium. (a) Microvessel segment, endometrial gland, (b) simple and (c) branched tubular, (d) single layer of columnar epithelium, (e) secretory material. Subepithelial surface (ES) and Basal endometrium (BE). Scale bar = 100 μm.

the luminal epithelial surface (b). Each of these networks arises as an extension of a single spiral arteriole. In this projection, there are four terminal vessels arising from different spiral arterioles (c) and traveling parallel to each other towards the inner surface of the luminal epithelium. The distance between each arteriolar extension appears to be approximately 30 μm.

Another orthogonal projection of early secretory phase endometrium, Fig. 4, shows a small block of tissue which measures 100 μm × 562 μm × 562 μm, and a total volume of 0.032 mm^3 and is representative of an area approximately 150 μm below the epithelial surface. The individual segment lengths of capillary endothelial cells that make up the inter-branching portions of a microvessel (red) are clearly distinguishable (a). The microvessels can be seen branching around the glandular structures, and appear to be remarkably uniform in shape and diameter throughout the section. There is regular and even branching in all directions between individual microvessels, in contrast to the microvessels in Fig. 3 which appear to be traveling predominantly in one direction. The total number of separate microvascular structures observed in the volume fraction of tissue illustrated in Fig. 4 was 63 with an average length of each variable segment being 71 μm (range 23–233 μm, ± SD 54). The total number of microvascular structures observed branching was 27, with an average inter-branching distance of 51 μm (range 17–128 μm, ± SD 29) at an average angle of 66° (range of 60–140°, ± SD 35). The total number of acute angles observed was 21 at an average angle of 55° (range 10–82°, ± SD 21), the total number of right angles observed was 1, and the total number of obtuse angles observed was 5 at an average angle of 117° (range 102–150°, ± SD 21). The distribution of these lengths, inter-branching distances and their angles are presented in Figs. 5–7. The ability to apply a numerical assessment to these distributions allows the possibility of very detailed assessment of abnormal vascular patterns.

The endometrial glands (green) in Fig. 4 appear to be fairly tortuous and this is consistent with being at a depth of 150 μm below the epithelial surface during the early

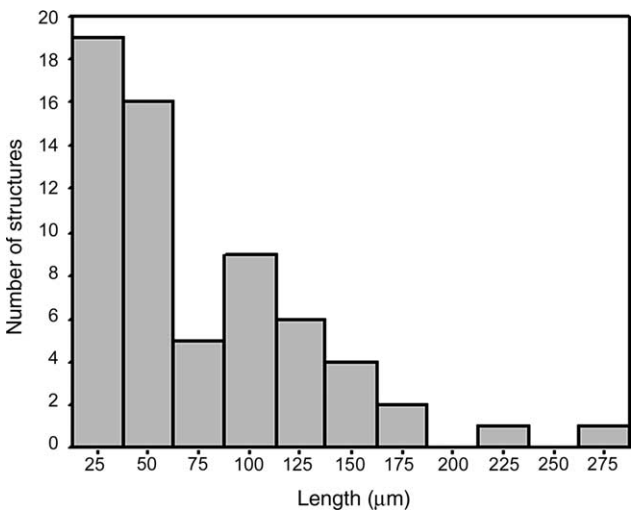

Fig. 5. Distribution of microvascular segment lengths in early secretory phase endometrium.

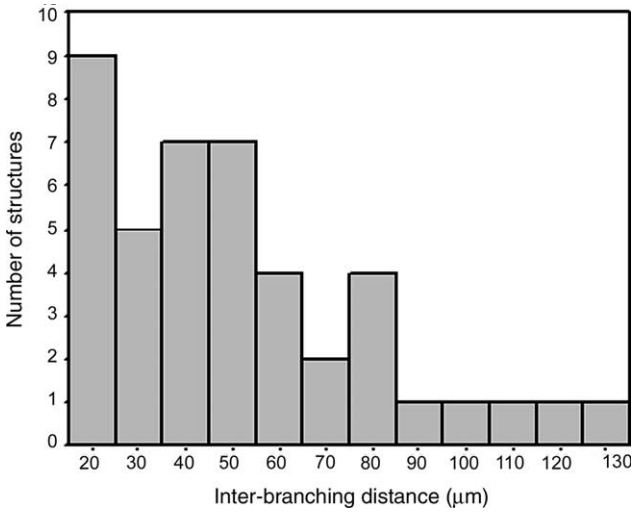

Fig. 6. Distribution of microvascular inter-branching distances in early secretory phase endometrium.

secretory phase. The endometrial glands appear to have both simple (b) and branched tubular shapes (c). Clearly visible within the endometrial glands is the single cell layer of the columnar epithelium (d). The glandular lumen contains secretory material, typically mucus, glycogen, proteins or lipids, which is shown by green diffuse staining (e). There is no clear pattern of microvascular relationships around the endometrial glands although a partial network is sometimes visible.

The structural detail of the glands and vessels in Figs. 3 and 4 suggests that pretreatment of the tissue with sodium deoxycholate and then with pepsin in HCl, has not significantly altered the tissue and cellular architecture.

A further orthogonal projection is Fig. 8, using the raw data sets obtained for Fig. 4, and the third party visualization software ImarisBasic 3.1 has allowed a shadow projection. The same level of morphological detail can be seen, as in Fig. 4, ImarisBasic 3.1 not only allowed for a morphological

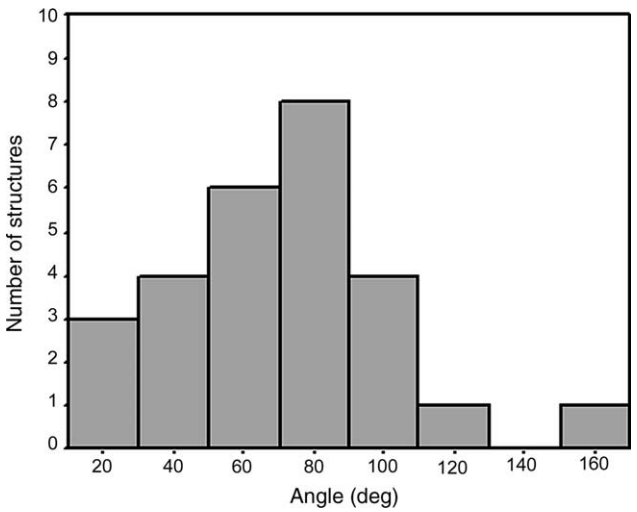

Fig. 7. Distribution of microvascular branching angles in early secretory phase endometrium.

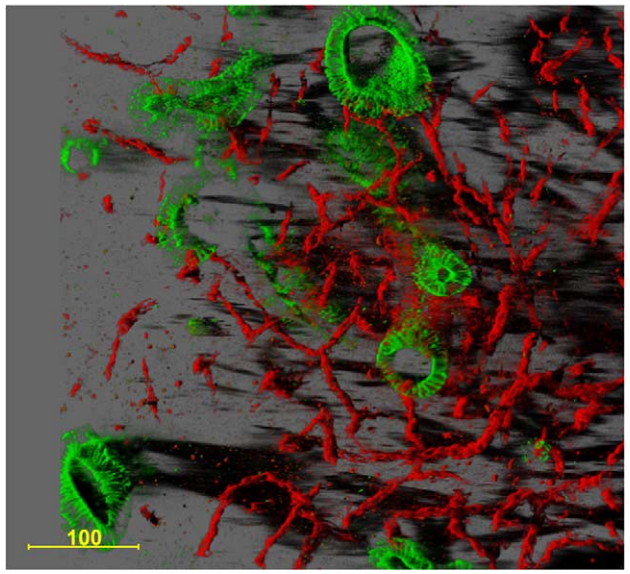

Fig. 8. An orthogonal projection, using the same raw data sets as Fig. 4, illustrating the microvascular (red) and glandular structures (green) in endometrium with shadow projection. Scale bar = 100 μm.

assessment, has also numerous tools for the further preparation of data. One function is a threshold cut-off this allowed for the background noise to be removed, and left all the other data intact resulting in a somewhat more 'skeletonised' projection. The visualization output mode selected for displaying the 3D rendered image was 'Blend'. When using this mode the colour obtained is shown by blending all the values along the viewing direction and including their transparency. Another visualization effect within blend is the lighting feature, if it is activated it will result in a shadowing effect such as in Fig. 8. By using this software package we were able to 'remove' the loose and dense stromal cells and connective tissue, in order to demonstrate individual microvessels more clearly.

4. Discussion

In this preliminary study, we have combined whole-mount/thick sections and MPE microscopy to scan endometrial tissue blocks to a depth of 100–120 μm. This produced a series of high resolution, low background images and removed the need for section registration/alignment that had been required by previous techniques (Manconi et al., 2001). This method has enabled a more accurate insight into the 3D relationships of the endometrial microvascular and glandular structures than has been previously possible. This has made it a very useful tool for demonstrating capillary networks, their size and shape, the relationship between groups of cells, and between structures. It has also offered the ability to perform accurate morphological assessments on small structures within a moderate volume of tissue.

Three-dimensional imaging by MPE has demonstrated well developed endometrial microvascular networks and their relationship with endometrial glandular structures in early secretory phase endometrium. The microvessels formed distinctive morphological patterns, straight vessels that parallel each other, parallel vessels that cross-link, incompletely closed loops (arcs), arcs with branching (Fig. 4). This methodology was able to elucidate the distribution and interaction between structural components in terms of their true 3D nature, and allow derivation of measurements of individual length, inter-branching distance and angles. The ability to derive such data will enable us to compare the relationships between microvessels and other structures in the endometrium, throughout normal and abnormal menstrual cycles and also further our investigation of abnormal bleeding in users of hormonal contraception and hormone replacement therapy.

In early secretory phase endometrium, the glandular growth outstrips that of the stroma and the glands thus become progressively more convoluted (Fig. 4). The most obvious and best documented changes in endometrium during the menstrual cycle occurs, in the endometrial glands during the secretory transformation after ovulation. These changes include glandular development from a relatively simple tubular state in the proliferative phase through a remarkably coordinated series of steps of growth and secretion in the secretory phase (Dockery et al., 1988; Dockery and Rogers, 1989).

Another feature of MPE is the ability to produce Second Harmonic Generation (SHG). SHG is a second order nonlinear optical process (Gauderson et al., 2001) and only arises when the molecule of interest lacks a centre of symmetry. It can produce 3D images of the collagen in cellular membranes and intact tissues without the use of exogenous labels (Campagnola et al., 2001). This approach has enabled us to image the distribution of collagen within endometrium in relation to other components (Cox et al., 2002, 2003) and will be valuable in combination with labels to simultaneously image glands and microvessels, as demonstrated in this paper.

5. Conclusion

This paper has described a novel visualization technique that demonstrates the usefulness of MPE and molecular probes to isolate both vascular and glandular structures within the endometrium during its monthly cyclic development. The ability to optically scan at 0.2 μm intervals through a maximal depth of 120 μm in the uterine tissue allowed for a greater degree of slice registration and the potential for 3D imaging. The need for artificial fiducial markers was found to be greatly minimized unless a depth greater than 120 μm was required; this has been met with structures being anatomically accurate and a noticeable reduction in labour intensiveness when compared to other optical serial reconstruction methods. Future developments of the technology will include a software based application to derive quantitative data from the volume rendering in order to obtain length and diameter of microvascular and glandular segments.

Acknowledgements

We thank Professor Peter Russell, Head of Anatomical Pathology, Royal Prince Alfred Hospital, Sydney, Australia, Dr Patrick Schwarb, Bitplane AG Scientific Solutions, Zurich, Switzerland, Dr Allan Jones, Electron Microscope Unit, University of Sydney, Dr Gavin Dixon, Department of Pathology, University of Sydney, Mr Darryl Cameron, Department of Anatomy and Histology, University of Sydney, Mr Lawrence Young, DAKO Corporation, Australia.

References

Bartelmez, G.W., 1933. Histologic studies on the menstruating mucous membrane during menstruation. Contributions to Embryology 142, 142–157.

Blackwell, P.M., Fraser, I.S., 1981. Superficial lymphatics in the functional zone of normal human endometrium. Microvascular research 21, 142–152.

Blackwell, P.M., Fraser, I.S., 1988. A morphometric and ultrastructural study of the microvessels of the functional zone of normal human endometrium with some notions on possible secretory functions of the endothelial cells. Asia-Oceania Journal of Obstetrics and Gynaecology 14, 233–250.

Campagnola, P.J., Clark, H.A., Mohler, W.A., 2001. Second-harmonic imaging microscopy of living cells. Journal of Biomedical Optics 6, 277–286.

Cox, G., Manconi, F., Kable, E., 2002. Second harmonic imaging of collagen in mammalian tissue. Proceedings of SPIE—The International Society for Optical Engineering 4620, 148–156.

Cox, G., Kable, E., Jones, A., Fraser, I.S., Manconi, F., Gorell, M.D., 2003. 3-Dimensional imaging of collagen using second harmonic generation. Journal of Structural Biology 141, 53–62.

Denk, W., Strickler, J.H., Webb, W.W., 1990. Two-photon laser scanning fluorescence microscopy. Science 248, 73–76.

Dockery, P., Rogers, A.W., 1989. The efforts of steroids on the fine structure of the endometrium. Baillieres Clinical Obstetrics and Gynaecology 3, 227–247.

Dockery, P., Li, T.C., Rogers, A.W., Lenton, E.A., Cooke, I.D., Warren, M., 1988. An examination of the variation in the timed endometrial biopsy. Human Reproduction 3, 715–720.

Dockery, P., Perret, S., Rogers, P.A.W., Bulut, E.H., Rea, B., Warren, A.M., Li, C.T., Harvey, B.J., Jenkins, D., Cooke, I.D., 2000. In: O'Brien, P.M.S., Cameron, I.T., MacClean, A.V. (Eds.), Disorders of the Menstrual Cycle, RCOG Press, London, pp. 43–55.

Ferenczy, A., 1994. In: Kurman, R.J., (Ed.), Blaustein's Pathology of the Genital Tract, Springer, New York, pp. 327–366.

Gauderson, R., Lukins, P.B., Sheppard, C.J.R., 2001. Optimization of second-harmonic generation microscopy. Micron 32, 691–700.

Gerritsen, H.G., De Grauw, C.J., 1999. Imaging of optically thick specimen using two-photon excitation microscopy. Microscopy Research and Technique 47, 206–209.

Lee, L.M., Hashimoto, H., Kusakabe, M., 1997. A note on the preparation of whole mount samples suitable for observation with the confocal laser scanning microscope. Acta Histochemica 99, 101–109.

Livingstone, M., Fraser, I.S., 2002. Mechanisms of abnormal uterine bleeding. Human Reproduction Update 8, 60–67.

Manconi, F., Markham, R., Cox, G., Kable, E., Fraser, I., 2001. Computer-generated, three-dimensional reconstruction of histological parallel serial sections displaying microvascular and glandular structures in human endometrium. Micron 32, 449–453.

Markee, J.E., 1940. Menstruation in intraocular endometrial transplants in the rhesus monkey. Contributions to Embryology 28, 220–318.

Noyes, R.W., Hertig, A.T., Rock, J., 1950. Dating the endometrial biopsy. Fertility and Sterility 1, 3–25.

Peticolas, W.L., Goldsborough, J.P., Rieckhoff, K.E., 1963. Double photon excitation in organic crystals. Physical Review Letters 10, 43–45.

Ramsey, E.M., 1989. In: Wynn, R.M., (Ed.), Biology of the Uterus, Plenum Press, New York, pp. 57–68.

Simbar, M., Manconi, F., Markham, M., Hickey, M., Fraser, I.S. A three-dimensional study of endometrial microvessels in women using the subdermal levonorgestrel implant system, Norplant. Submitted for publication.

Simón, C., Caballero-Campo, P., Galan, A., Martin, J.C., Meseguer, M., Herrer, R., Valbuena, D., Jasper, M., Mercader, A., 2002. In: Glasser, S.R., Aplin, J.D., Giudice, L.C., Tabibzadeh, S. (Eds.), The Endometrium, Taylor & Francis, London, pp. 194–207.

Smith, S.K., 2002. In: Glasser, S.R., Aplin, J.D., Giudice, L.C., Tabibzadeh, S. (Eds.), The Endometrium, Taylor & Francis, London, pp. 73–85.

Straub, M., Hell, S.W., 1998. Multifocal multiphoton microscopy: a fast and efficient tool for 3-D fluorescence imaging. Bioimaging 6, 177–185.

Wilson, T., Sheppard, C.J.R., 1984. Theory and Practice of Scanning Optical Microscopy, Academic Press, London.